A record of spontaneous subduction initiation in the Izu-Bonin-Mariana arc

Richard J. Arculus, Osamu Ishizuka, Kara A. Bogus, Michael Gurnis, Rosemary Hickey-Vargas, Mohammed H. Aljahdali, Alexandre N. Bandini-Maeder, Andrew P. Barth, Philipp A. Brandl, Laureen Drab, Rodrigo do Monte Guerra, Morihisa Hamada, Fuqing Jiang, Kyoko Kanayama, Sev Kender, Yuki Kusano, He Li, Lorne C. Loudin, Marco Maffione, Kathleen M. Marsaglia, Anders McCarthy, Sebastién Meffre, Antony Morris, Martin Neuhaus, Ivan P. Savov, Clara Sena, Frank J. Tepley III, Cees van der Land, Gene M. Yogodzinski, Zhaohui Zhang

Author's version of Supplemental Materials for:

Arculus, R. J., Ishizuka, O., Bogus, K. A., Gurnis, M., Hickey-Vargas, R., Aljahdali, M. H., … Zhang, Z. (2015). A record of spontaneous subduction initiation in the Izu-Bonin-Mariana arc. Nature Geoscience, 8(9), 728–733. http://doi.org/10.1038/ngeo2515

Contents

S1 Seismic cross-sections

The two-way travel times recorded by seismic reflection for the crossing lines D98-A and D98-08 (Fig. 2) through Site U1438 are shown in Figure S1.

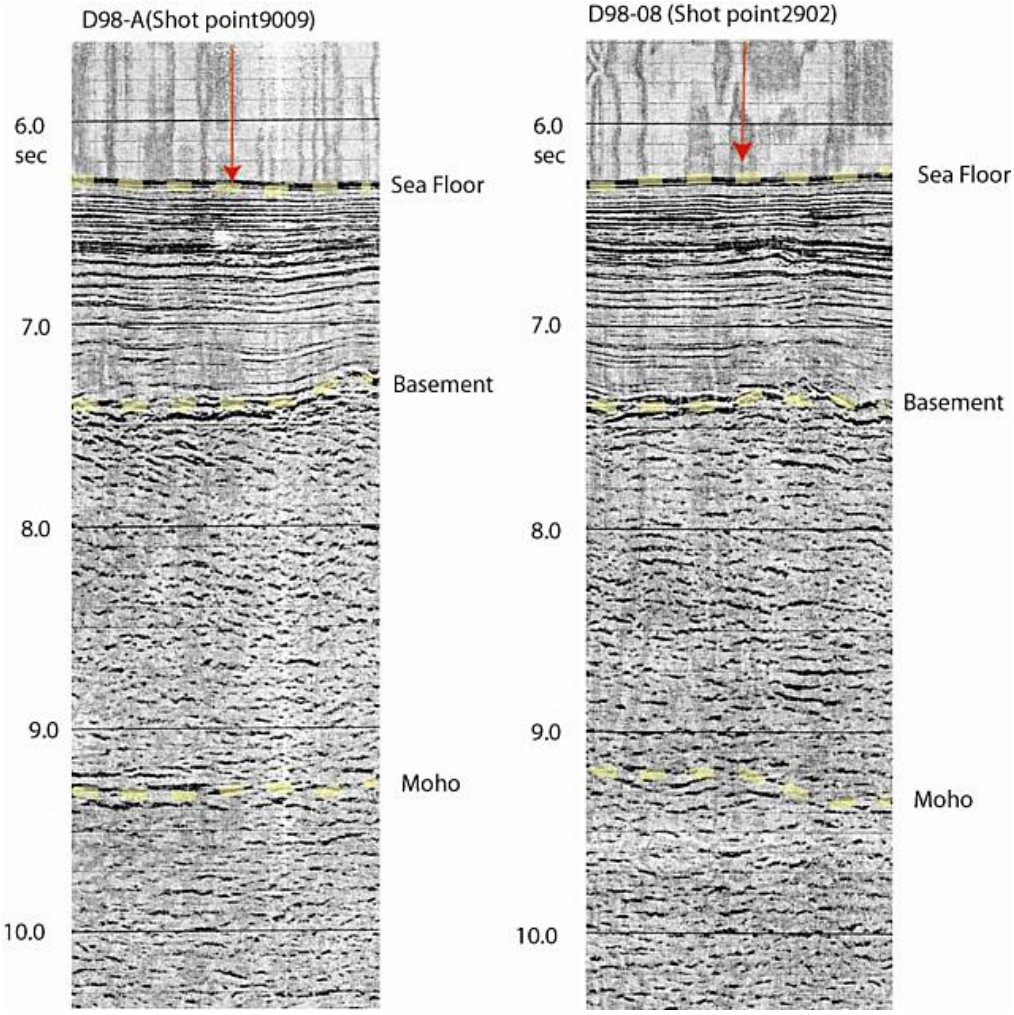

Figure S1. Details of the multi-channel seismic profiles (see Fig. 2 for location) that intersect at Site U1438. An estimate of the sediment-igneous basement interface and Moho location is indicated by yellow dashed lines. The vertical axis is two-way travel time in seconds.

S2 Petrology of Unit 1

The majority of phenocrysts in basalts of Unit 1, which comprises the Amami Sankaku Basin basement and lowermost lithostratigraphic unit of Site U1438, range in size from 0.2 to 4 mm. Plagioclase phenocryst abundances range from 0% to 30%, although 0–5%

is predominant. The phenocrysts tend to be blocky and sometimes zoned. Clinopyroxene phenocrysts occur more rarely and tend to be smaller (0.2 mm) than plagioclase. The occurrence of olivine either as phenocrysts or in the groundmass is difficult to estimate due to strong alteration. Some olivine pseudomorphed by chlorite is recognizable by shape and the presence of small, partially translucent, reddish chrome spinel inclusions. The visible alteration consists predominantly of patchy chlorite and oxides replacing phenocrysts and groundmass, chlorite and carbonate filling sparse vesicles, and veins filled with chlorite + carbonate ± sulfides and/or oxides. Vesicles are present in approximately one-third of the studied rocks but are usually sparsely distributed within each. The groundmass of the basalts is mostly holocrystalline and is composed primarily of plagioclase, clinopyroxene, and titanomagnetite. Glass can be significant in the groundmass (up to 85%; average = 25%), but is entirely altered mostly to chlorite. Representative photomicrographs are shown in Figure S2.

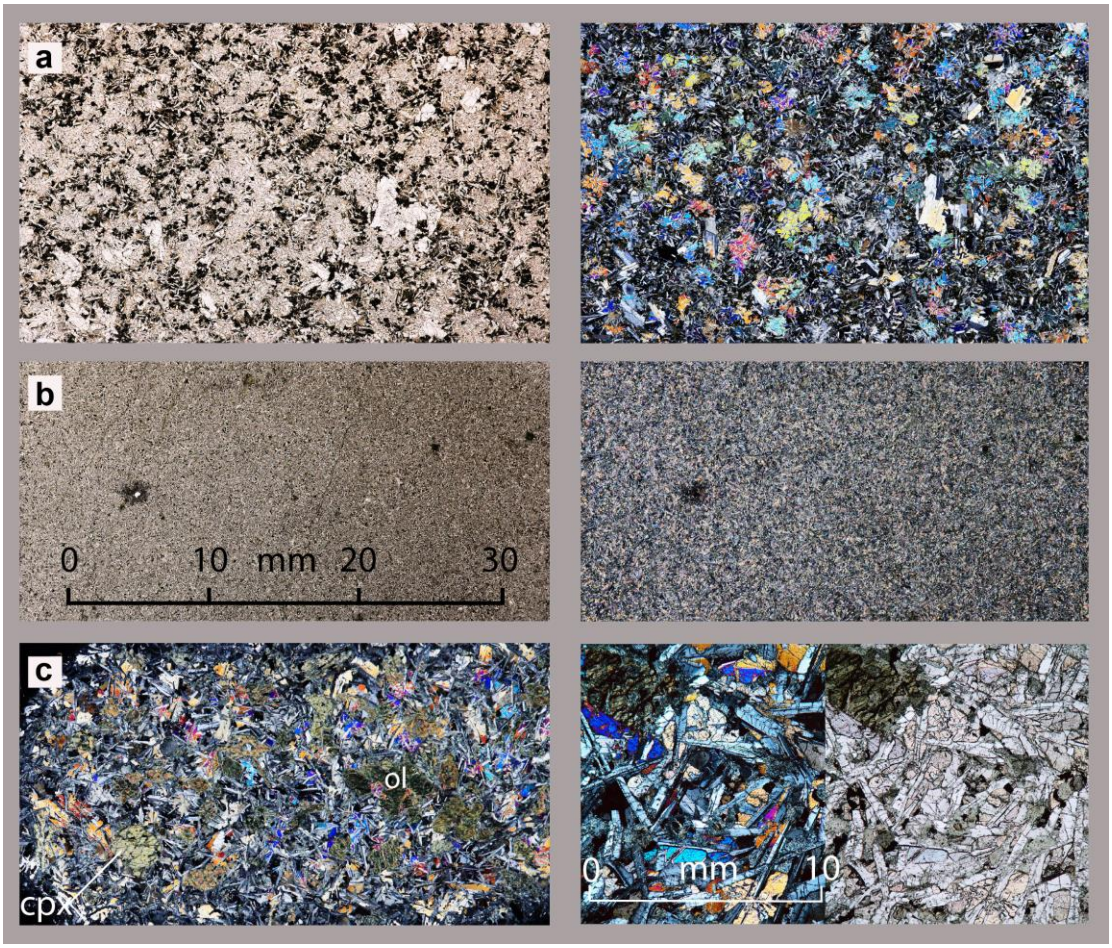

Figure S2. Whole thin section and detailed photomicrographs of Site U1438E Unit 1 basalts showing different textural types: a) fine-grained basalt with ophitic texture (351-U1438E-78R-2); b) aphyric microcrystalline basalt (351-U1438E-77R-3); For a and b,

views on the left are in plane polarized light and on the right are cross-polarized light. Horizontal dimension of the fields in all images except in bottom right panel is shown by the scale bar in (left). c) fine- to medium-grained basalt with ophitic texture, clinopyroxene (cpx) and altered olivine phenocrysts (ol) (351-U1438E-80R-1) on left, and details of same thin section on right with cross-polarized (left) and plane polarized (right). Scale bar is for both left and right of this image pair.

S3 Analytical Techniques for Shipboard ICP-AES

Thirty-seven samples from the Unit 1 basalts were collected (Cores U1438E-70R to 88R) and analyzed for major and trace elements by inductively coupled plasma–atomic emission spectroscopy (ICP-AES; Table S1). The majority of these samples are high-MgO (mostly >8 wt%), low-TiO_2 (0.6–1.1 wt%) tholeiitic basalts.

Samples (~2-8 cm^3) were cut from the core with a diamond saw blade with cut surfaces ground on a diamond-impregnated disk. The samples were cleaned ultrasonically in a beaker containing trace-metal-grade methanol (15 min), followed by deionized water (10 min), and then Barnstead deionized water (18 MΩ·cm; 10 min). The cleaned pieces were dried for 10–12 h at 110°C and then crushed (<1 cm chips) between two Delrin plastic disks in a hydraulic press. The chips were ground to a fine powder using a SPEX 8515 Shatterbox with a tungsten carbide lining. An aliquot of sample powder was weighed (1000.0 ± 0.5 mg) and then ignited (700°C for 4 h) to determine weight loss on ignition (LOI). Ignited powders for each sample and standard were weighed (100.0 ± 0.2 mg; Cahn C-31) and mixed with $LiBO_2$ flux (400.0 ± 0.5 mg; pre-weighed on shore). Weighing errors were estimated as ±0.05 mg under relatively smooth sea surface conditions. Aqueous LiBr solution (10 mL of 0.172 mM) was then added to the flux and powder mixture as a non-wetting agent. Samples were fused individually in Pt-Au (95:5) crucibles for ~12 min at a maximum temperature of 1050°C in an internally rotating induction furnace (Bead Sampler NT-2100). The beads were transferred into high-density polypropylene bottles, dissolved in a solution of 10% HNO_3 and 10 ppm Ge (50 mL), and shaken on a Burrell wrist-action shaker (1 h). Solution increments (20 mL) were passed through a filter (0.45 µm) into a clean high-density polypropylene bottle. From the filtered solution, 1.25 mL was pipetted into a scintillation vial and diluted with 8.75 mL of a

dissolution solution containing 10% HNO_3. The final solution-to-sample dilution factor is 4000:1.

Major (Si, Ti, Al, Fe, Mn, Mg, Ca, Na, K, and P) and trace (Sc, V, Cr, Sr, Y, Zr, Ba) element concentrations of samples and standards were measured on a Teledyne Leeman Labs Prodigy ICP-AES instrument using multiple wavelengths commonly selected for silicate rocks, and instrument-specific start-up and peak search routines. Data were acquired using Gaussian peak fitting; each sample and standard was analyzed in quadruplicate within a given sample run. A 10% HNO_3 rinse solution was used (90 sec) between analyses. Thirteen certified rock standards (AGV-2, BCR-2, BHVO-2, GSP-2, JB-2, JG-2, JG-3, JP-1, JR-1, JR-2, Nod-A-1, STM-1, VS-N) were used. Standard JB-2 is from the Izu-Bonin Arc, so it was analyzed as an unknown. Each run consisted of the standards interspersed with blanks and the samples in quadruplicate. Standard JR-2 was analyzed at the beginning and end of each run and interspersed in the sequence for instrument drift correction. Measured raw-intensities were corrected offline for instrument drift using the shipboard "ICP Analyzer" software. A linear calibration line for each element was calculated using the standards from which element concentrations in the samples were determined from relevant calibration lines. Calibration standards were analyzed in quadruplicate and yielded a precision of Al < 0.4%, Ca < 0.6%, Fe < 0.5, K < 0.6%, Mg < 0.5%, Mn < 0.6, Na < 1.5, Si < 0.4%, and Ti < 0.5%, Ba < 1.5%, Cr < 6.6%, Sr < 0.9%, Sc < 1.6%, V < 9.7%, Y < 1.0%, and Zr < 1.7%. For major elements, data were rejected if volatile-free weight percentages totals were outside 100±5 wt% and are reported normalized to 100 wt% total. Blank solutions aspired during each run were below detection limits for all elements.

In addition to the data presented in Figure 4, we show equivalent plots (Figs S3 and S4) incorporating previously published analytical data for samples recovered by De Bari et al.[22], at location A on Figure 1 (proposed to be equivalent to FAB[24]), and the 159 Ma samples recovered at location B on Figure 1[23].

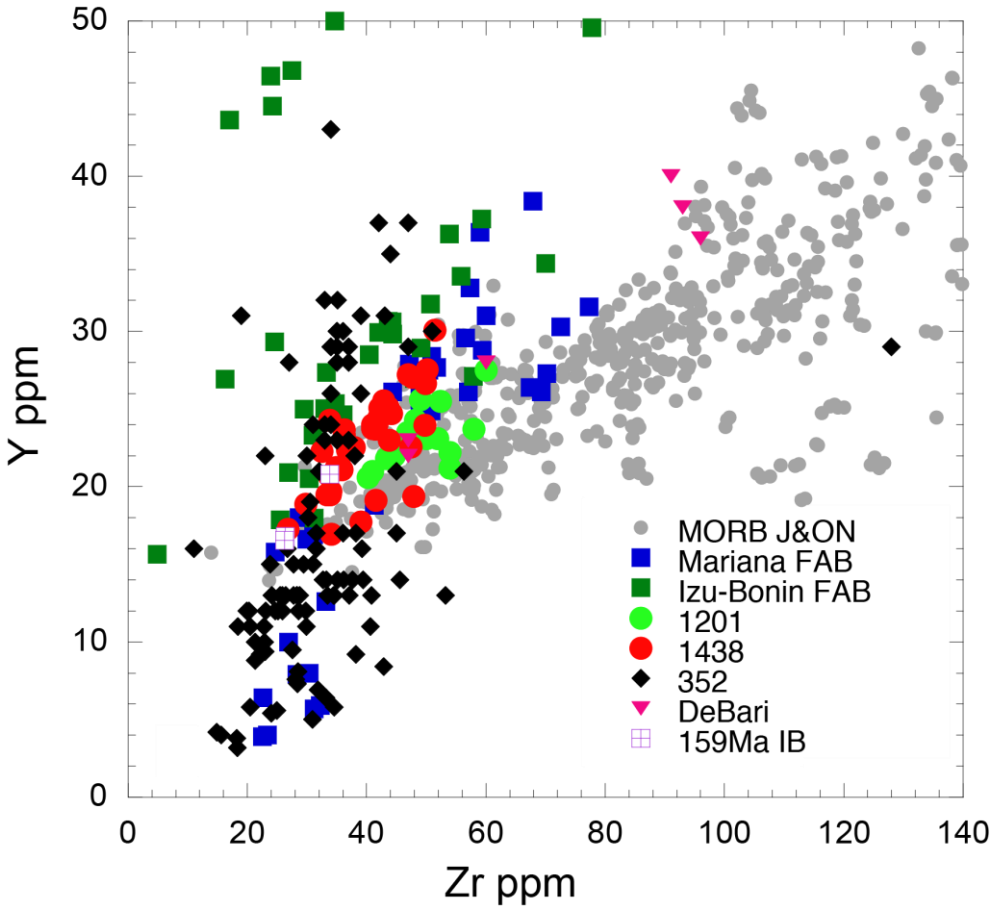

Figure S3. Comparison of Zr vs Y concentrations for samples from De Bari et al.[22] and 159 Ma basalts from the IBM forearc[23] with global MORB[29], Izu-Bonin-Mariana fore-arc basalts (FAB)[23,24], Site 1201[21], Site U1438, IODP Expedition 352 FAB and boninite[26].

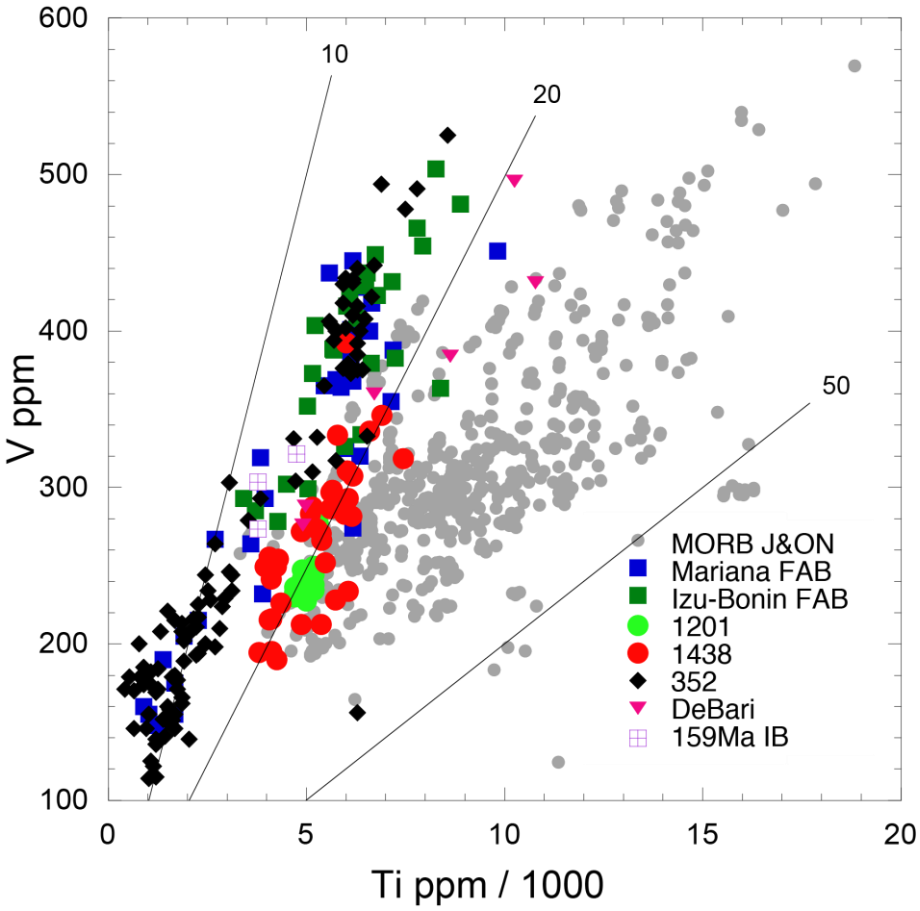

Figure S4. Comparison of V vs Ti concentrations for samples from De Bari et al.[22] and 159 Ma basalts from the IBM forearc[23] with global MORB[29], Izu-Bonin-Mariana fore-arc basalts (FAB)[23,24], Site 1201[21], Site U1438, IODP Expedition 352 FAB and boninite[26]. Most MORB have 20< (Tippm/1000)/Vppm <50 whereas tholeiitic basalts in island arcs, including FAB, have (Tippm/1000)/Vppm<20[36]. Some boninite from the Izu-Bonin-Mariana arcs have (Tippm/1000)/Vppm<10[26].

Table S1. Analytical results for samples from Unit 1, Site U1438

S4 Details of Unit IV lithology and paleontology

The lithology at Site U1438 consists of sediments, sedimentary rocks, and igneous rocks (Fig. 3). Sediments and sedimentary rocks at Site U1438 were recovered from the seafloor to 1461 meters below seafloor (mbsf) and are divided into four lithostratigraphic units. Unit I (160.3 m thick) is recent to latest Oligocene in age and the sediments are primarily terrigenous, biogenic, and volcaniclastic mud and ooze with interspersed discrete ash layers. Unit II (139.4 m thick) is Oligocene in age and the sedimentary rocks are tuffaceous mudstone, siltstone, and fine sandstone with

localized slumping-induced deformation features. The mudstone to sandstone intervals are typically normally-graded beds with sharp lower boundaries to the sandstone bases, as well as moderately to strongly bioturbated mudstone caps. Unit III (1046.4 m thick) is Oligocene to Eocene in age; the sedimentary rocks are generally coarser grained than those of Unit II and include tuffaceous mudstone, tuffaceous sandstone, tuffaceous medium to coarse sandstone with gravel, and tuffaceous breccia-conglomerate with volcanic and sedimentary clasts commonly up to pebble and (rarely) cobble size. At the largest scale, Unit III comprises five intervals of coarser clastic sedimentary rocks, separated by intervening mudstone-dominant intervals lacking discrete breccia-conglomerate beds. Unit IV (99.7 m thick) and is Eocene in age. It is composed of radiolarian-bearing mudstone underlain by medium to coarse sandstone, breccia-conglomerate, and tuffaceous siltstone and mudstone. The centimeter- to decimeter-scale layers of sandstone range in color from dark greenish gray to very dark gray, and exhibit normal grading, lamination, and cross lamination. These intervals consist of common to abundant volcanic rock fragments exhibiting microlitic to vesicular to pumiceous textures, in addition to rounded to subangular grains of plagioclase, pyroxene, amphibole, and opaque minerals. There are some black, tachylitic glass fragments with plagioclase microlites. Siltstone/mudstone fragments are rare. The feldspar, ferromagnesian minerals, and volcanic grains are variably altered to zeolites and clay minerals (which also occur as cementing phases), although clinopyroxene grains are mostly unaltered. Alteration minerals include chlorite-clay, zeolite, hematite, and titanite. In the sandstones 10 m above basement, laminae are unusual in that they are crystal-rich (predominantly plagioclase and green amphibole) with amphibole-bearing, felsic groundmass volcanic fragments. Three high-Na basaltic andesite sills intrude the sediments between 49–55 m above the basement. The sills are sparsely phyric, with 3%–5% phenocrysts and microphenocrysts of clinopyroxene (0.2–1.0 mm) set in a groundmass of devitrified glass with microlites of plagioclase and pyroxene. The sole presence of clinopyroxene phenocrysts distinguish the sills from basalts of the underlying basement. There is no evidence in the oldest sediments for a large component of clastic material derived from uplifted subjacent basement as expected from induced subduction. There is also no evidence for any intense regional deformation of the sediments other than some minor faulting. Unit IV is underlain by igneous basement rocks comprising Unit 1 (See Section S1 for characteristics).

Radiolaria are present in the 4 m-thick mudstone and sandstone section above basement, but are nondeterminable in age. The oldest sample yielding determinable radiolaria is 40 m above basement (Fig. S5). The assemblage contains radiolarian genera characteristic of the latest Paleocene–early Eocene. Based on the presence of *Buryella* spp., *Phormocyrtis* spp., *Podocyrtis* spp., and *Theocotylissa* spp., the age of the sample is tentatively interpreted as latest Thanetian–Ypresian (RP7 [top]–9; 56.83–48.57 Ma). A sandy sample from Section 66R-CC, 12 m above basement, contains two specimens of very poorly preserved, partially recrystallized planktonic foraminifers. One specimen probably belongs to the species *Acarinina bullbrooki* (Zones E7–E11; 50.2–40.49 Ma), or possibly *Acarinina soldadoensis* (Zones P4c–P9; 57.79–44.49 Ma)[1](Fig. S6).

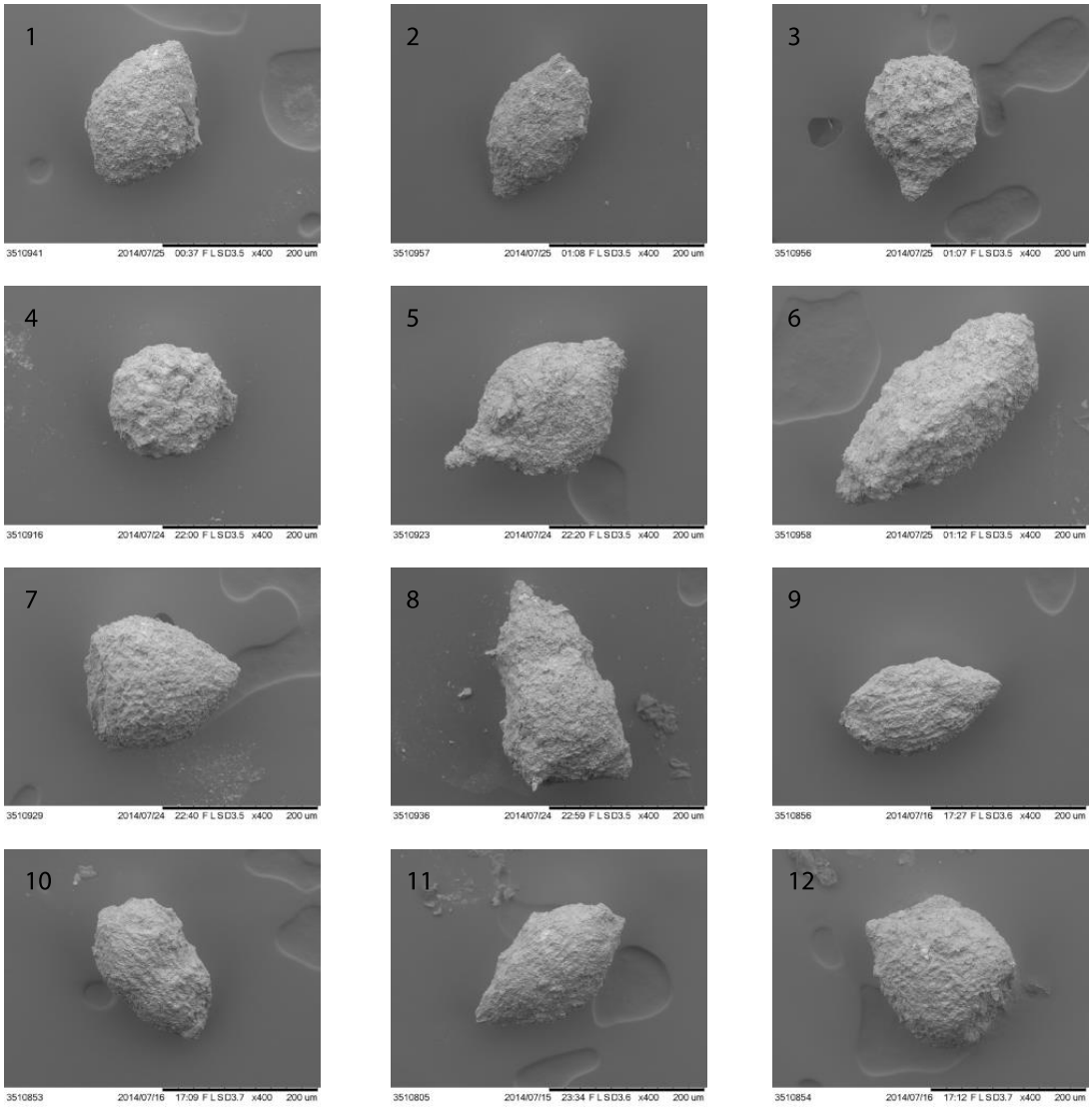

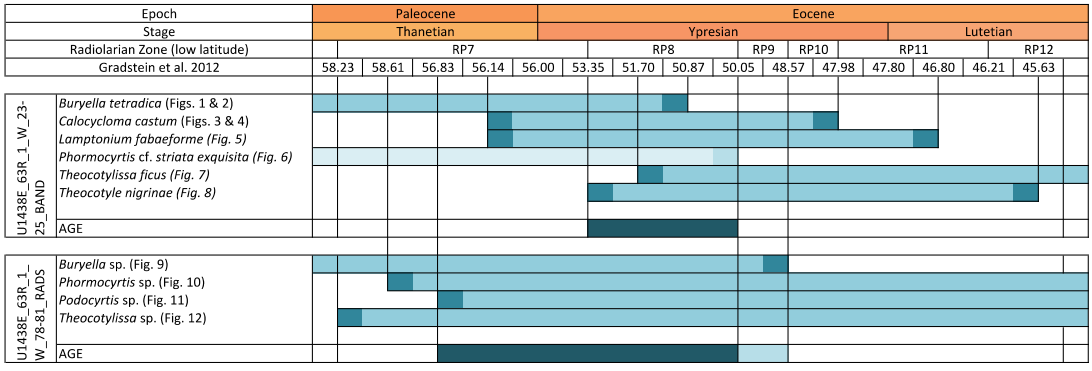

Figure S5. Scanning electron microscope images of radiolarians from Unit IV of Site U1438 and genera ranges used to constrain the age (lower panel). Sample U1438E-63R-1W, 23-25 cm (Early Eocene): 1 and 2. *Buryella tetradica*; 3 and 4. *Calocycloma castum*; 5. *Lamptonium fabaeforme*; 6. *Phormocyrtis* cf. *striata exquisita*; 7. *Theocotylissa ficus*; 8. *Theocotyle nigrinae*. Sample U1438E-63R-1W, 78-81 cm

(latest Paleocene-Early Eocene): 9. *Buryella* sp.; 10. *Phormocyrtis* sp.; 11. *Podocyrtis* sp.; 12. *Theocotylissa* sp.

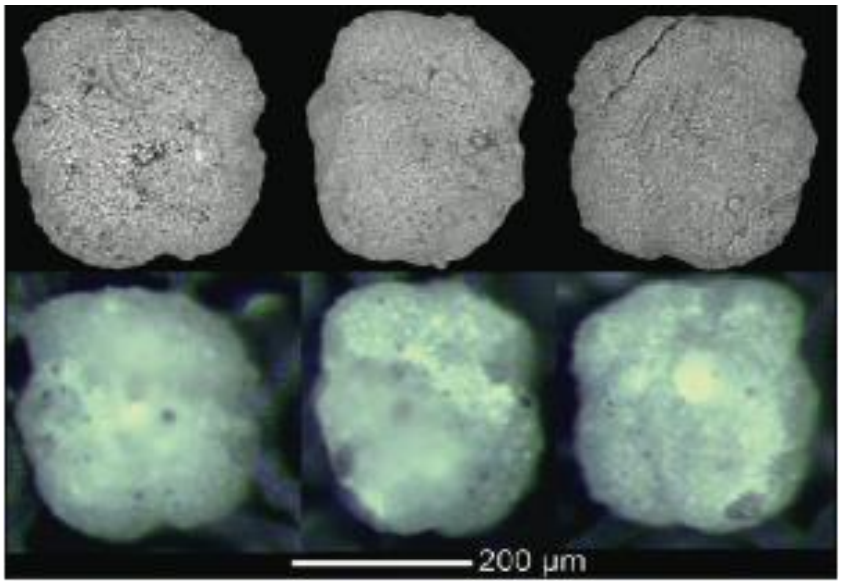

Figure S6. Scanning electron microscope (upper) and reflected light (lower) images of *Acarinina* sp. from Sample U1438E-66R-CC.

S5 Downhole temperature, thermal conductivity, heat flux, water depth and thermal age

Successful temperature measurements were made at seven depths using the advanced piston corer temperature tool (APCT-3)[2] from the mudline to 83.2 mbsf. The temperatures as a function of depth did not show any substantial deviation from a linear geothermal gradient of 77.6°C/km (Fig. S7). Thermal conductivity was measured using the Teka TK04 system by transient heating of the sample with a known heating power and geometry[3]. Changes in temperature with time during heating are recorded and used to calculate thermal conductivity. At these depths, the sediment was poorly consolidated, so a needle probe was inserted into the sediment through a 2 mm hole, drilled into the plastic core liner, to measure the thermal conductivity. All measurements were subsequently corrected for *in situ* conditions using the method of Hyndman et al.[4] in which the temperatures were determined from the interpolated APCT-3 measurements (Fig. S7a). Spurious values with $k_s < 0.85$ W/[m·K] from each set of three individual measurements were removed and the mean and standard deviation determined. Overall, there were 28 measurements of the core approximately evenly spaced down to 100 mbsf. The measurements did not vary

substantially from a constant value of 0.951±0.046 W/mK (Fig. S7b). A combination of the temperature measurements with the thermal conductivity using Bullard-type analysis[5] indicated the thermal gradient did not change with depth in the upper part of Site U1438 (Figure S7c). This suggests a geotherm that is undisturbed by local processes, such as sediment compaction, fluid flow within the porous sediments, or internal heat production from radioactive decay. With these measured thermal conductivities, the calculated heat flux is 73.7 mW/m^2 (Figure S7d). The intersection of the measured heat flux with the empirical plate age-reliable heat flow relation[25] occurs at 50 Ma. Given the range of the individual heat flow values and uncertainty in basement age for each reliable heat flow value, a conservative estimate for the thermal age of the ASB is 40-60 Ma. This estimate is independent of the use of a plate model or a half space model when interpolating between reliable heat flow values.

A preliminary estimate of the sediment load–corrected depth of the basement at Site U1438 gives a depth of ~5527 m. A residual depth of ~550 m is calculated from an expected depth of 5000 m for a 50 Ma age plate[6]. This is consistent with other estimates for the west Philippine Sea Plate and within the range observed for the Shikoku and Parece Vela basins, which have excess depths of 500–1000 m[7]. In other words, the entire region around Site U1438 has water depths greater than predicted by the average subsidence of the sea floor and is interpreted as a dynamic draw-down by mantle flow. The water depths suggest that the age of the plate might be slightly younger than the 50 Ma thermal age, but, at a minimum, the heat flux and water depth give ages consistent with that inferred from biostratigraphy.

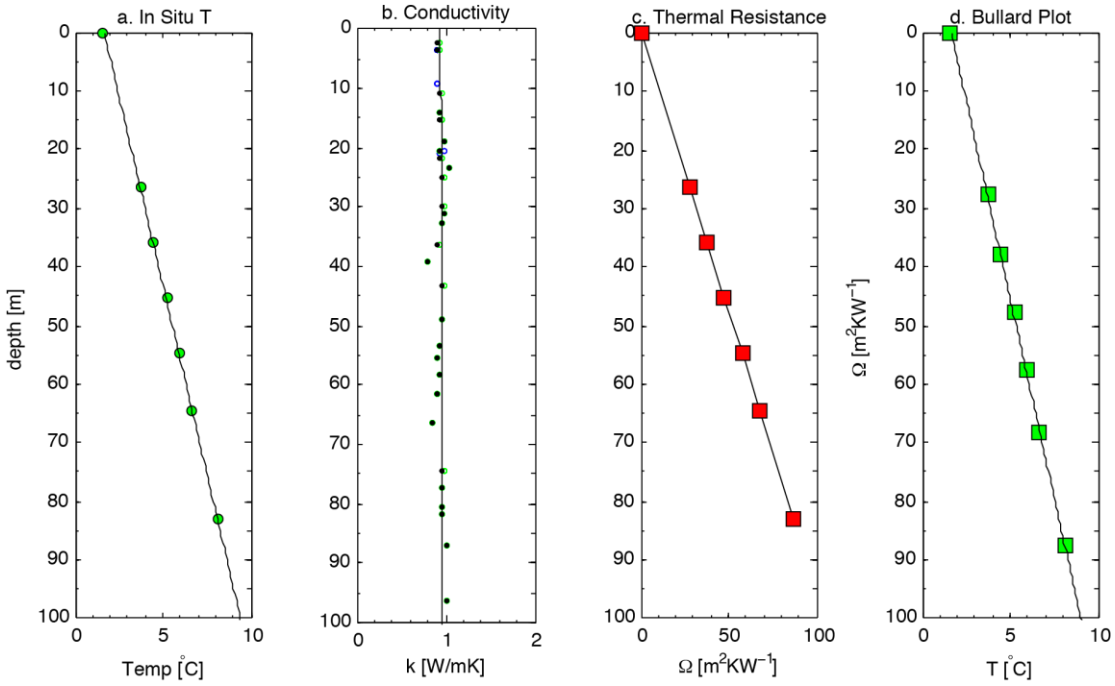

Figure S7. Temperature gradient, conductivity, thermal resistance, and Bullard plot for data obtained with the advanced piston corer temperature tool at Site U1438.

References

1. *Pearson*, P.N., *et al.* Atlas of Eocene *Planktonic F*oraminifera. Cushman Foundation for Foraminiferal Research, Fredericksburg, USA, Cushman Foundation Special Publication **41** 513 pp (2006).
2. Heesemann, M. et al. Data report: testing and deployment of the new APCT-3 tool to determine in situ temperatures while piston coring. *Proc. Integrated Ocean Drill. Program* **311**, 1–19, doi:10.2204/iodp.proc.311.108. (2006).
3. Blum, P. Physical properties handbook. *ODP Tech. Note*, 26. doi:10.2973/odp.tn.26. (1997).
4. Hyndman, R.D. et al. Geothermal measurements on DSDP Leg 26. *Proc. DSDP Init. Repts.* **26**, 451-463 (1974).
5. Bullard, E.C. Heat flow in South Africa. *Proc. R. Soc. London A* **173**, 474-502 (1939).
6. Sclater, J.G., Jaupart, C. & Galson, D. The heat flow through oceanic and continental crust and the heat loss of the Earth. *Revs. Geophys. Space Phys.* **18,** 269-311 (1980).
7. Winterbourne, J., White, N. & Crosby, A. Accurate measurements of residual topography from the oceanic realm. *Tectonics* **33**, 982-1015 (2014).